Materials Physics and Mechanics. 2022;48(3): 367-378
Research article
http://dx.doi.org/10.18149/MPM.4832022_7

Submitted: October 13, 2021
Approved: May 5, 2022
Accepted: May 12, 2022

Preparation and characterization of undoped and antimony doped tin oxide thin films synthesized by spray pyrolysis

H. Habieb, N. Hamdadou✉

Laboratoire de Micro et de Nanophysique (LaMiN), Ecole Nationale Polytechnique d'Oran Maurice AUDIN, BP 1523 El Mnaouer, Oran 31000, Algeria

✉ nasreddine.hamdadou@enp-oran.dz

Abstract. Undoped and antimony doped tin oxide thin films (SnO_2 :Sb) have been deposited by the spray pyrolysis method on glass substrates heated at 350°C, with various doping concentrations 0 (undoped), 1 at.%, 3 at.%, and 5 at.%. The influence of annealing temperature and various Sb doping rates on the structural, morphological and optical properties have been investigated, using grazing incidence X-ray diffraction (GIXRD), profilometry, atomic force microscopy (AFM), UV-Visible spectrophotometry and photoluminescence measurements (PL). GIXRD diagrams show that the films deposited at various Sb concentrations are polycrystalline with a tetragonal rutile type structure and preferred orientation direction along [110]. It has been also noted that the grain size changes between 11 nm and 25 nm. Atomic force microscopy (AFM) visualization revealed that surface morphology was found to be influenced by the incorporation of Sb and average roughness was varied between 4.580 nm and 10.793 nm. The optical characterization shows that the maximum value of transmittance of 82 % was found for SnO_2: 1 at.% Sb thin films were annealed at 400°C for 4 hours and the optical band gap values range from 3.668 eV to 4.224 eV of SnO_2 films. Room-temperature photoluminescence measurements under excitation at 325 nm show broad emission peak, Photoluminescence (PL) properties influenced by antimony doping for the SnO_2 films are investigated.

Keywords: Transparent Conducting Oxide (TCO), Antimony Doped Tin Oxide Thin Films, Spray Pyrolysis, Annealing Temperature, Grazing Incidence X-ray Diffraction (GIXRD), Profilometer, Atomic Force Microscopy (AFM), Photoluminescence (PL)

Acknowledgements*. The authors are thankful to LABMAT Laboratory of National Polytechnic School of Oran (ENPO-MA-), Algeria, for the AFM and PL characterization of our samples.*

Citation: Habieb H, Hamdadou N. Preparation and characterization of undoped and antimony doped tin oxide thin films synthesized by spray pyrolysis. *Materials Physics and Mechanics*. 2022;48(3): 367-378. DOI: 10.18149/MPM.4832022_7.

1. Introduction

Transparent conducting oxides (TCO) like In_2O_3, SnO_2, ZnO, In_2O_3: Sn … etc have been the subject of research over a number of years due to their promising properties. Tin oxide SnO_2 is a n-type semiconductor with a wide bandgap E_g = 3.6 eV at 300K [1], and electrical resistivity varying from 10 to 10^6 Ωcm, depending on the temperature and the stoichiometry of the oxide [2]. In the thin films form, SnO_2 is a transparent material, characterized by high

optical transmission in the visible range ~90, these properties make it very attractive for several applications, like solar cells, optoelectronic devices, thin-film resistors, antireflection coatings, photochemical devices, electrically conductive glass. SnO_2 material is usually used in the field of monitoring air pollution and toxic gas detection [3]. Doped and undoped SnO_2 thin films have been prepared by various techniques such as sol-gel [4-6], reactive radio frequency sputtering (RF) [7], direct current (DC) magnetron sputtering [8], electron beam evaporation [9] and spray pyrolysis [10-12].

In the present study, SnO_2 thin films are deposited by employing a spray pyrolysis technique. We are principally interested in this chemical technique for its advantages like ease of adding dopant material, reproducibility, high growth rate, and mass production capability for uniform large area coatings, which are desirable for industrial, solar cell, and gas sensors applications. We have made an attempt to synthesize pure and Sb doped SnO_2 thin films on glass substrates by the chemical spray pyrolysis technique and the influence of annealing temperature and antimony dopant concentration on the structural, morphological and optical properties of the prepared films is reported.

2. Experimental methods

Thin films preparation. The substrates of dimensions 7.6 cm × 2.6 cm × 0.1 cm were carefully initially cleaned chemically, by keeping in distilled water, acetone and ethanol individually each for 5 min. These substrates were further treated ultrasonically with pure water for 9 min to remove surface contamination and dried at room temperature. The substrates were preheated to the required temperature, prior to deposition.

Undoped and antimony doped tin oxide thin films were deposited on glass substrates by using a spray pyrolysis system HOLMARC Model HO-TH-04. The chemical reagents used were stannous (II) chloride dihydrate ($SnCl_2.2H_2O$, 97%, BIOCHEM Chemopharma, Quebec Canada) and antimony trichloride ($SbCl_3$, 99%, BIOCHEM Chemopharma, France) as host and dopant precursors. Initially, 0.1M of $SnCl_2.2H_2O$ and $SbCl_3$ solutions were made separately by dissolving in appropriate amounts of deionized water and methanol CH_3OH volume proportion: 13 ml: 13 ml with adding a few drops of hydrochloric acid HCl to obtain a standardized and transparent working solution. Then the solution was prepared by mixing the existing solutions in appropriate volume ratios, to obtain the targeted concentrations 0 at.%, 1 at.%, 3 at.% and 5 at.% of Sb doped SnO_2 thin films. The solution was stirred continuously at room temperature for 15 min until it became transparent and homogeneous. After that, the resulting solution was sprayed on the glass substrate at an optimized substrate temperature of 350°C with an accuracy of ± 1°C for 10 min with a compressed air pressure of 2 bars. The normalized distance between the spray nozzle and the substrates, the flow rate, and the total quantity of spray solution were 12 cm, 200 µl/min, and 30 ml respectively. During the spraying, the nozzle moved with longitudinal and transverse speeds $v_x = 400$mm/s and $v_y = 8$ mm/s respectively. The substrate's temperature was maintained using a digital temperature controller. After deposition, the films were annealed in a programmable tubular oven under air and with a heating rate of 10°C/ min at temperatures 400°C, 450°C, 500°C, and 550°C for 4h.

Thin films characterization. A set of complementary investigation methods has been used to characterize the thin films prepared. The structural analysis has been carried out by Inel EQUINOX 3000 diffractometer using grazing incidence X-ray diffraction (GIXRD) with Cu-Kα radiation, λ = 1.54056Å at room temperature in the scan range of 2θ between 20° and 90°, continuously with the step width of 0.03° and a fixed incidence angle of 5°. The thickness of all the films was estimated by BRUKER Dektak XT profilometer with standard scan type. The morphology of the films was examined by atomic force microscope (AFM) Nano surf C3000 in tapping mode at room temperature. The optical properties of the deposited films are

measured in the wavelength region of 190-1100 nm of the spectrum at room temperature using spectrophotometer SPECORD 210 Plus UV/VIS/IR. Also, we made a complementary investigation using the room temperature photoluminescence (PL), the films were analyzed by spectrometer HORIBA iHR-550 equipped with CCD detector (400–1000 nm) and the InGaAs detector (800–1600 nm). The He-Cd laser of wavelength 325 nm (UV) or equivalently at energy 3.815 eV and power of 30mW was used as the excitation source.

3. Results and discussion

Structural properties. The GIXRD patterns obtained for undoped and doped SnO_2: Sb thin films at doping rates 0 (undoped) and 5 at.% before and after annealing at temperatures 400°C, 450°C, 500°C, and 550°C, are shown in Figs. 1 and 2 respectively.

GIXRD diffractograms recorded on pure SnO_2 thin films with different annealing temperatures deposited at a substrate temperature of 350°C using 0.1 M stanic chloride are shown in Fig. 1. All the peaks in the pattern correspond to tetragonal rutile structure of SnO_2 and are indexed on the basis of ICCD file N° 00-41-1445. It is quite clear from the GIXRD diagrams that all the films are polycrystalline and highly oriented along (110) plane, this result corresponds to those reported by several works [13,14]. Presence of other plane orientations such as (101), (200), (211), (220), (310) and (301) have also been detected [15,16]. Although the intensities of all peaks increase with increasing annealing temperatures, this is related to the increase in the rate of SnO_2 crystallites, this result is in perfect agreement with the work of S. Laghrib et al. [17].

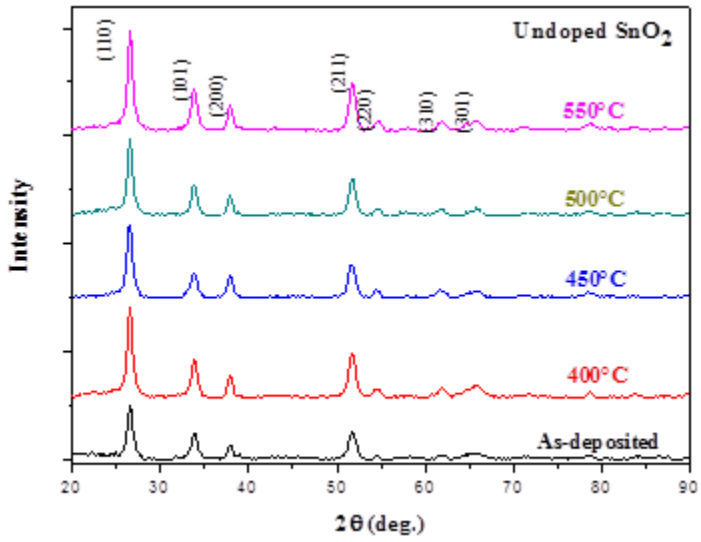

Fig. 1. GIXRD patterns of undoped SnO_2 thin films before and after annealing at different temperatures

The GIXRD patterns of as-deposited and annealed Sb-doped SnO_2 thin films are shown in Fig. 2 for 5 at.% of Sb doping rate. It can be seen, that the produced films are polycrystalline and all the diffractograms contain the characteristic SnO_2 peaks only. No phase corresponding to antimony, antimony oxides, or any other antimony compound was detected in the GIXRD patterns, which indicates that O atoms were replaced by Sb atoms in the SnO_2: Sb thin films. The (110) peak is the strongest peak observed for all the films. The addition of dopants does not affect the preferred [110] orientational growth of the films, the same result was observed by Junji S. et al. [18].

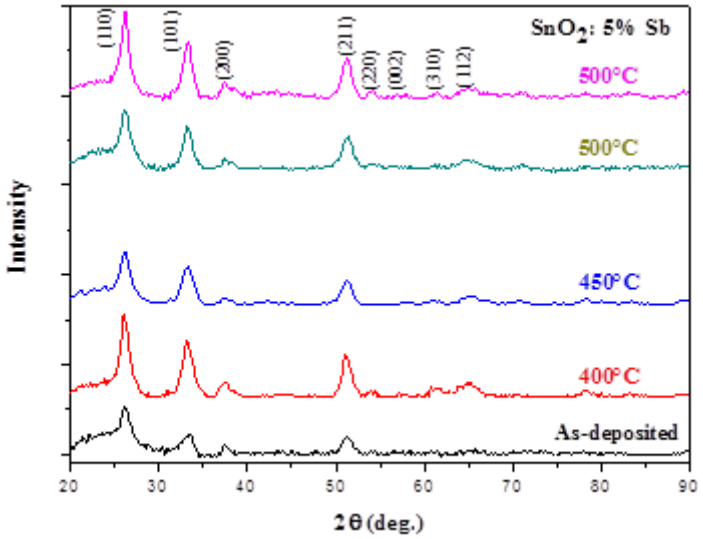

Fig. 2. GIXRD patterns of SnO_2: 5 at.% Sb thin films before and after annealing at different temperatures

Table 1 shows the GIXRD parameters: mean grain size D (nm), the preferred orientation plane $F_{hk0}(\%)$, lattice parameters a and c (Å), and crystalline structure, of undoped and antimony doped SnO_2 thin films with various concentrations of 0 (undoped), 1 at.%, 3 at.%, and 5 at.% for different annealing temperatures.

The lattice parameters a and c of the identified structure were calculated by Eq. (1), where (hkl) is the lattice plane:

$$\frac{1}{d_{hkl}^2} = \frac{h^2+k^2}{a^2} + \frac{l^2}{c^2}. \quad (1)$$

The lattice parameters values presented in Table 1 are in good agreement with those given in ICDD card N° 00-41-1445. The mean grain size D of thin films was also calculated, using the Scherrer formula based on GIXRD patterns [19,20]:

$$D = K\frac{\lambda}{\beta cos\theta}. \quad (2)$$

In which K = 0. 9, λ = 1.54056 Å is the wavelength of the incident radiation, θ is the Bragg angle and β is the full width at half maximum (FWHM) of the diffraction peak. β was calculated by the Warren relation [21]:

$$\beta^2 = B^2 - b^2, \quad (3)$$

where B is the measured peak width and b = 0.08° is the instrumental peak broadening, due to the instrument of GIXRD. The mean grain sizes of the samples were found between 11nm and 25nm.

The degree of preferential grain orientation according to $(hk0)$ plane was determined using the following equation:

$$F_{hk0} = \frac{\sum I(h,k,0)/I_0(h,k,0)}{\sum I(h,k,l)/I_0(h,k,l)}, \quad (4)$$

where $I(hkl)$ is the measured intensity of X-ray diffraction, $I_0(hkl)$ is the corresponding standard intensity from the ICDD data. The degree of preferential orientation according to the plane $(hk0)$ of SnO_2: 3 at.% Sb thin films is in the order of 44%.

Morphological Properties. The thin films of undoped and Sb doped SnO_2 at 1 at.%, 3 at.% and 5 at.% respectively, annealed at 400 °C for 4h were examined by the AFM device to characterize the surface roughness. The AFM measurements are carried out in the air in "tapping mode". Figure 3 displays the 2D and 3D AFM images of Sb-doped SnO_2 thin films annealed at 400 °C with a Sb concentrations of 0 (undoped) and 5 at.% obtained over an area of 2 × 2 μm^2.

Table 1. GIXRD parameters and mean grain size of undoped and antimony doped SnO_2 thin films with various Sb concentrations of 0 (undoped), 1 at.%, 3 at.%, and 5 at.% for different annealing temperatures

Doping rate	T_a (°C)	Crystalline structure	a, c (Å)	D (nm)	F_{hk0} (%)
0 at.%	As-prepared	Tetragonal	a = 4.740 c = 3.204	23	64
	400				
	450				
	500				
	550				
1 at.%	As-prepared		a = 4.766 c = 3.195	25	53
	400				
	450				
	500				
	550				
3 at.%	As-prepared		a = 4.780 c = 3.293	11	44
	400				
	450				
	500				
	550				
5 at.%	As-prepared		a = 4.740 c = 3.204	14	43
	400				
	450				
	500				
	550				

The average roughness R_a and the root mean square R_q (RMS) parameters were calculated from AFM data using the following relations:

$$R_a = \frac{1}{l}\int_0^l |Z(x)|dx, \tag{5}$$

$$R_q = \sqrt{\frac{1}{l}\int_0^l Z^2(x)dx}, \tag{6}$$

where $Z(x)$ is the function, that describes the surface profile, analyzed in terms of height Z and position x of the sample over the evaluation length l. The results are collected in Table 2, with thickness values measured by a profilometer as a function of Sb doping.

All samples show a polycrystalline morphology, and the grain size gradually decreases with an increase of Sb concentration. The grain size is seen to be larger than the crystallite size estimated from XRD measurements; however, this is also attributable to the agglomeration of smaller crystallites. Also, we see from the AFM images, a trend of

formation of nanostructures in the form of aggregate with different sizes in relation to doping concentration. It has been suggested that there is homogeneous granulates on all surfaces of the films, these results are in very good agreement with previous works [18]. The root mean square (RMS) surface roughness values for samples with Sb concentrations of 0 (undoped) and 1 at.%, 3 at.%, and 5 at.% were found to be 7.707 nm and 13.563 - 5.725 - 8.334 nm, respectively.

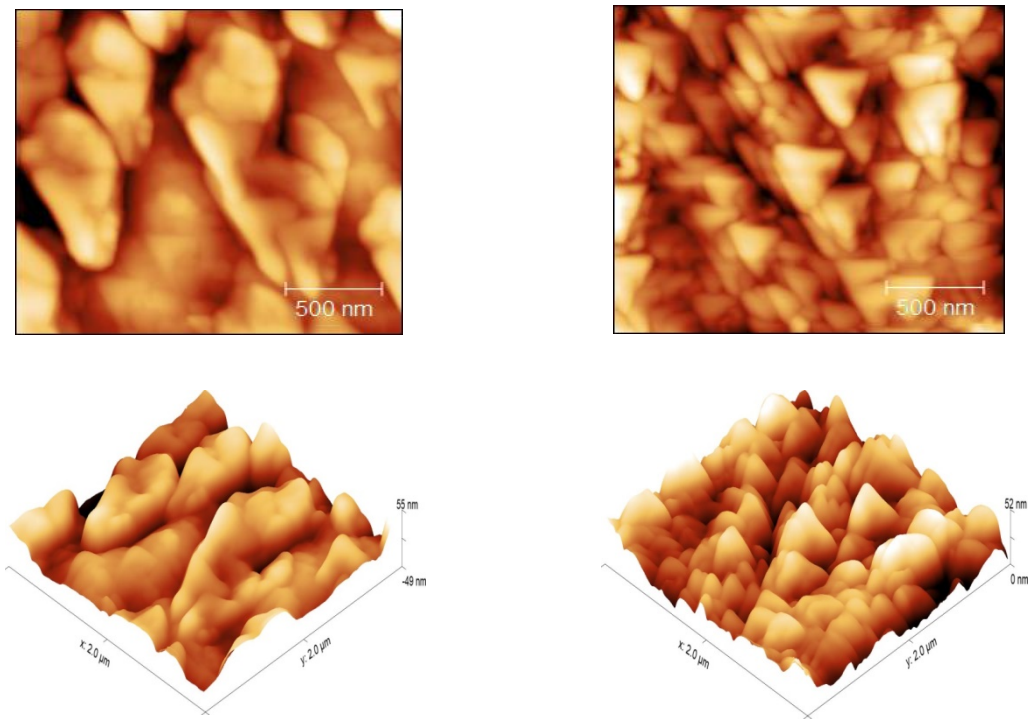

(a) **(b)**

Fig. 3. 2D and 3D AFM images of Sb-doped SnO_2 thin films annealed at 400°C with Sb concentration of 0 (undoped) (a) and 5 at.% (b)

Table 2. Surface roughness parameters and thickness of undoped and Sb doped SnO_2 thin films annealed at 400°C for 4h

Sb-doping concentration (at. %)	Thickness (nm)	R_a (nm)	R_q (nm)
0	340	5.709	7.704
1	155	10.793	13.563
3	141	4.580	5.725
5	306	6.694	8.334

Optical properties. Figure 4 shows the optical transmittance of the undoped and Sb doped SnO_2 thin films and those deposited at Sb doping concentration 5 at.%, in the wavelength range from 300 to 900 nm.

All the undoped SnO_2 thin films deposited have an average transmittance in the visible range that varies between 58% and 65%, it has been noticed that this transmittance increases with the increase of annealing temperature. The increased transparency observed may be attributed to less scattering effects and better crystallinity.

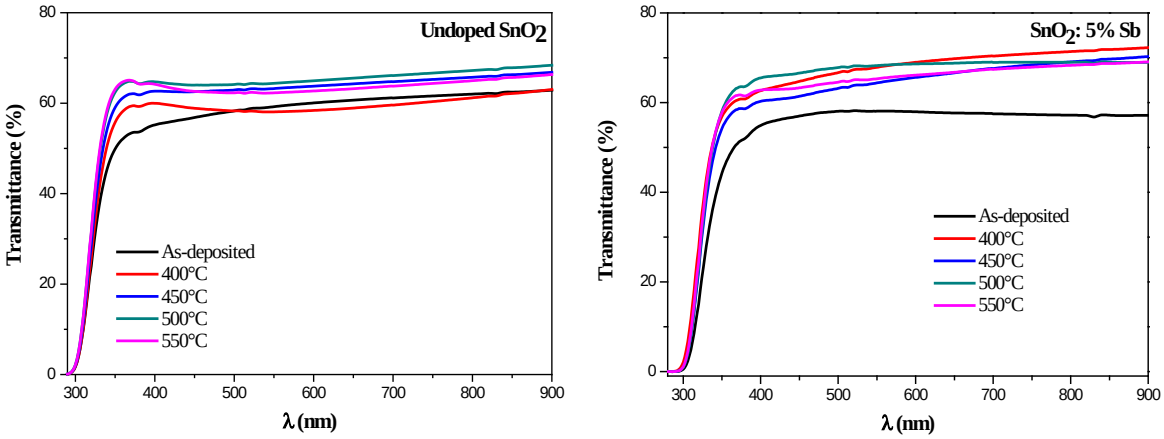

(a) **(b)**

Fig. 4. Optical transmittance spectra of undoped (a) and Sb doped SnO_2 thin films before and after annealing at different temperatures (b)

We have noticed that transmittance increases after doping with 1 at.%, 3 at.% and 5 at.% Sb, and all the films display high transmittance in the visible and near-infrared ranges. It indicates that the highest optical transmittance is of the order of 82% for SnO_2: 1 at.% Sb thin films annealed at 400°C for 4h.

From the transmission spectra and the thickness determined by the profilometer, we calculate the absorption coefficients α using the following relation:

$$\propto = \frac{1}{e}\ln\left(\frac{100}{T(\%)}\right), \quad (7)$$

where e is the film thickness.

In the low-energy region of the incident photon [1.5–3.5 eV], we notice a decrease in the absorption coefficient. It is clear that the rate of doping reduces the absorption coefficient.

Optical band gap E_g is an important characterization tool for thin film. The optical band gap of undoped and Sb doped SnO_2 thin films were evaluated from Tauc's equation [22],

$$(\alpha h\vartheta) = A(h\vartheta - E_g)^n, \quad (8)$$

where A is a constant, h is the Plank's constant, ϑ is the frequency of incident photon and α is the absorption coefficient. In eq. (8) the exponent n indicates the nature of band transition, the value of n is taken as ½, for the direct allowed transition nature of undoped and Sb doped SnO_2 thin films. The E_g values of the films were measured, from extrapolation of the straight line region of the $(\alpha h\vartheta)^2$ versus $h\vartheta$ graph to intercept the $h\vartheta$ axis. The obtained values of optical band gaps of all the films are mentioned in the respective plots, Fig. 5.

The direct bandgap, determined by extrapolating the straight-line portions to the energy axis to $(\alpha h\vartheta)^2 = 0$, is found to be varied between 4.099 and 4.224 eV for pure SnO_2 thin film, which is comparable to the value of Eg = 4.119 eV reported for single-crystal SnO_2 [23], these gap energy values are larger than the value of 3.62 eV for the bulk SnO_2 due to the contribution of quantum size effect of the present SnO_2 thin film [24]. On the one hand, we notice a decrease in the width of the band gap after doping (approximately 3.9 eV for SnO_2: 1 at.% Sb), this variation can be explained by the Roth effect [25]. And on the other hand, the gap increases again with the increase of the doping rate (3 at. % and 5 at.% Sb), the gap increases following the Burstein Moss effect [26,27], also this increase may occur due to the replacement of Sn^{+4} with Sb^{+5}, which fills the lower energy levels of the conduction band inside the forbidden gap region that then causes the increased carrier concentration. However,

these results converge on previously published studies, Table 3, that show that doped SnO_2 thin films generally exhibit wider band gap energies on the order of 4 eV [28,29].

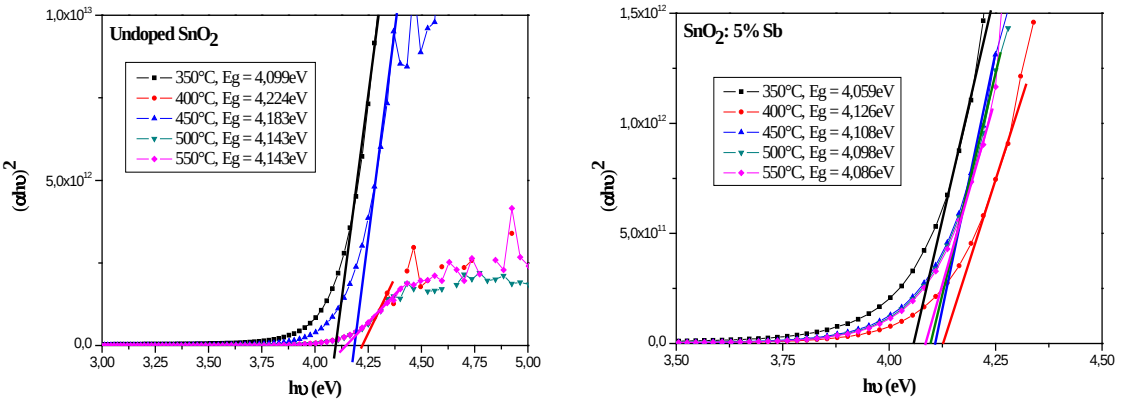

(a) **(b)**

Fig. 5. Plots of $(\alpha h\vartheta)^2$ vs. $h\vartheta$ of undoped (a) and Sb doped SnO_2 (b) thin films for different annealing temperatures

Table 3. Comparison of SnO_2 thin films band gap values

Thin films	Deposition method	Eg (eV)	References
Undoped SnO_2	Spray pyrolysis	4.09 - 4.22	Our study
	Spin coating	4.38	[30]
	Spin coating	4.10	[6]
	Ultrasonic spray pyrolysis	4.10	[31]
Sb doped SnO_2	Spray pyrolysis	4.10 – 4.12	Our study
	Radio-frequency magnetron sputtering	4.28 - 4.32	[32]
	/	4.17 - 4.41	[33]

Urbach energy, which characterizes crystalline disorder of films, can be determined by the following relation [34]:

$$\alpha = \alpha_0 \exp\left(\frac{h\vartheta}{E_u}\right), \quad (9)$$

where α_0 is a constant and E_u is the Urbach energy. The value of Urbach energy is calculated from the reciprocal value of the slope of the linear portion of $ln\alpha$ versus $h\vartheta$. We have found that for all the samples, the values of Urbach energy of undoped and doped SnO_2 films decreases from 0.286 eV to 0.283 eV, 0.319 eV to 0.299 eV, 0.319 eV to 0.305 eV and from 0.300 eV to 0.288 eV, for 0 at.%, 1 at.%, 3 at.% and 5 at.% Sb concentration, this result can be explained by the decrease in disorder in the films.

Photoluminescence (PL) analysis. Photoluminescence (PL) spectroscopy is a powerful technique for studying the behavior of SnO_2 luminescence as a function of Sb-doping content. We give in Fig. 6 the emission spectra for Sb-doped SnO_2 thin films annealed at 400°C with Sb concentration of 0 (undoped), 1 at.%, 3 at. % and 5 at.% obtained at room temperature normalized intensity recorded in the energy range (4.1–1.4 eV) corresponding to the wavelength range (~ 300–900 nm). For all the deposited thin films, the emission peaks have high intensity and are positioned at 359, 409, 535, and 718 nm. At room temperature, the high density of oxygen vacancies interacting with interfacial tin leads to the formation of a considerable amount of trapped states within the band gap, giving rise to high PL intensity. The peak at 359 nm (~3.45 eV) is sharp UV-violet luminescence peak, the visible region can

be split into three luminescence bands, peak at 409 nm is violet luminescence peak (~3.03 eV), peak at 534 nm is green luminescence peak (~2.32 eV) and peak at 718 nm (~1.73 eV) is red luminescence peak. According to the literature [35,36], the UV-violet is mainly generated by the electron transition from the donor level formed by oxygen vacancies (V_O) to the acceptor level formed by other defects and impurities. The UV-violet peak we observed from undoped SnO_2, and think that it is also due to oxygen vacancies (V_O). The UV-violet peak for the doped SnO_2 is due to the difference in the position of the donor level formed by Sb ions and oxygen vacancies (V_O). The violet can be related to tin interstitials and oxygen vacancies in the undoped SnO_2 thin films. For SnO_2: Sb films, the origin of the violet peak at 409 nm is attributed to the electron transition from the donor level formed by oxygen vacancies (V_O) or Sb^{+5} ions to the acceptor level formed by the Sb^{+3} ions [37]. In spray deposited polycrystalline oxides, oxygen vacancies are known to be the most common defects and form the donor level [38]. For our samples, because of the pyrolytic decomposition, there should be the existence of oxygen vacancies due to rapid evaporation and oxidation processes. A broad peak observed at 718 nm may be due to other crystal defects which are formed during the growth of samples. As to the origin of the peak at 535 nm of pure SnO_2 and Sb doped SnO_2, maybe it is related to other crystal defects which were formed during the growth of the samples, but it is not yet clear now.

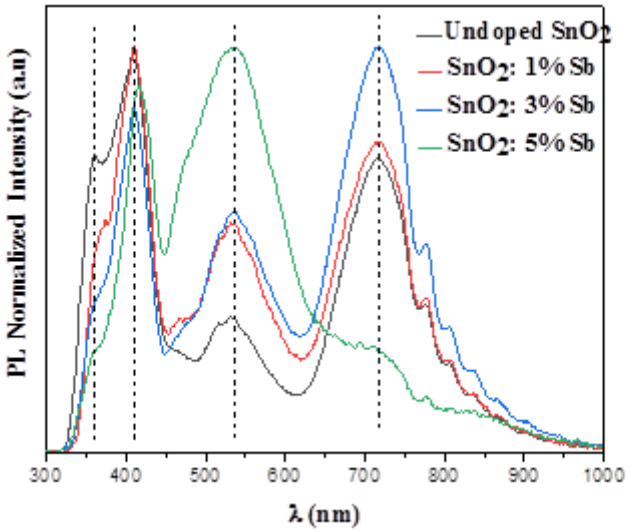

Fig. 6. PL emission spectrum of SnO_2 thin films with various Sb concentrations at excitation wavelength of 325 nm

4. Conclusion

In our study, transparent conducting SnO_2 thin films with different concentrations of Sb have been successfully fabricated on glass substrate by using the chemical spray pyrolysis technique. All the synthesized films are polycrystalline in nature and are matched with ICDD card number 00-41-1445 to confirm the tetragonal rutile structure of SnO_2 films. AFM measurements confirmed a polycrystalline rutile structure for all samples improved with XRD analysis and showed that the maximum roughness was noted for SnO_2: 1 at. % Sb thin films. The optical transmittance of the SnO_2 films increases with doping Sb. These results suggest that spray pyrolysis is a promising fabrication technique for TCOs films composed of Sb doped SnO_2. Strong violet emission has been seen in the luminescence spectra.

References

1. Chi-Fan L, Chun-Hsien K, Tao-Hsing C, Yu-Sheng H. Optoelectronic Properties of Ti-doped SnO_2 Thin Films Processed under Different Annealing Temperatures. *Coatings.* 2020;10(4): 394.
2. Saadeddin I, Pecquenard B, Manaud JP, Decourt R, Labrugère C, Buffeteau T, Campet G. Synthesis and characterization of single- and co-doped SnO_2 thin films for optoelectronic applications. *Applied Surface Science.* 2007;253(12): 5240-5249.
3. Hachoun Z, Ouerdane A, Bouslama M, Ghaffour M, Abdllaoui A, Caodano Y, Ali benamara A. Investigation of the properties of Sb doping on tin oxide SnO_2 materials for technological applications. *Materials Science and Engineering.* 2016;123: 012029.
4. Laxmikanta D, Prasanta KB. Synthesis and characterization of nanostructured Mn(II) doped antimony-tin oxide (ATO) films on glass. *Applied Surface Science.* 2013;280: 33-41.
5. Yuhua X, Shihui G, Li X, Yalu Z, Xueyun Z, Bangmin Z, Li Z, Chengxian L, Xiufeng H, Zhenchao W. Room temperature ferromagnetism of Mn-doped SnO_2 thin films fabricated by sol-gel method. *Applied Surface Science.* 2008;254(22): 7459-7463.
6. Belhamri S, Hamdadou N. Improved Properties of SnO_2 Thin Films Obtained Via Spin Coating Method by Varying the Solution Concentration. *Surface Review and Letters.* 2018;25(7): 1850092.
7. Chi-Fan L, Chun-Hsien K, Tao-Hsing C, Yu-Sheng H. Optoelectronic Properties of Ti-doped SnO_2 Thin Films Processed under Different Annealing Temperatures. *Coatings.* 2020;10(14): 394.
8. Morikawa H, Fujita M. Crystallization and electrical property change on the annealing of amorphous indium-oxide and indium-tin-oxide tin films. *Thin Solid Films*. 2000;359(1): 61-67.
9. Shamala KS, Murthy LCS, Narasimha RK. Studies on tin oxide films prepared by electron beam evaporation and spray pyrolysis methods. *Bull. Mater. Sci.* 2004;27(3): 295-301.
10. Kumar RR, Rao KN, Rajanna K, Phani AR. Novel co-evaporation approach for the growth of Sb doped SnO_2 nanowires. *Mater. Lett.* 2013;106: 164-167.
11. Zhang B, Tian Y, Zhang JX, Cai W. The Ftir studies of SnO_2:Sb(ATO) films deposited by spray pyrolysis. *Materials Letters.* 2011;65: 1204-1206.
12. Sushant G, Yadav BC, Prabhat KD, Das B. Microstructural, optical and electrical investigations of Sb-SnO_2 thin films deposited by spray pyrolysis. *Materials Research Bulletin.* 2013;48(9): 3315-3322.
13. Xu Y, Yamazaki M, Villars P. Inorganic materials database for exploring the nature of material. *Jpn. J. Appl. Phys*. 2011;50(11S): 11RH02.
14. Allag A, Saâd R, Ouahab A, Abdelmalek N, Brahim G. Effect of solution concentration on the structural, optical and electrical properties of SnO_2 thin films prepared by spray pyrolysis. *Optik*. 2015;127: 2653-2658.
15. Allag A, Saad R, Ouahab A, Attouche H, Kouidri N. Optoelectronic properties of SnO_2 thin films sprayed at different deposition time. *Chin. Phys. B.* 2016;25(4): 046801.
16. Bagheri-Mohagheghi MM, Shahtahmasebi N, Alinejad MR, Youssefi A, Shokooh-Saremi M. The effect of the post-annealing temperature on the nano-structure and energy band gap of SnO_2 semiconducting oxide nano-particles synthesized by polymerizing-complexing sol-gel method. *Physica B.* 2008;403(13-16): 2431-2437.
17. Laghrib S, Amardjia-Adnani H, Abdi1 D, Pelletier JM. Elaboration et étude des couches minces de SnO_2 obtenu par évaporation sous vide et recuites sous oxygène. *Revue des Energies Renouvelables.* 2007;10(3): 357-366.
18. Junji S, Tasuku K. Structural and electrical properties of Sb-doped SnO_2 thin films prepared by metal organic decomposition. *Thin Solid Films.* 2019;685: 210-215.

19. Klug HP, Alexander LE. *X-Ray Diffraction Procedures*. NY: John & Wiley and Sons; 1954.
20. Patterson AL. The Scherrer formula for X-ray particle size determination. *Phys. Rev.* 1939;56(10): 978.
21. Warren BE. X-ray diffraction methods *J. Appl. Phys.* 1941;12(5): 375.
22. Tauc J. Absorption edge and internal electric fields in amorphous semiconductors. *Mater. Res. Bull.* 1970;5(8): 721-729.
23. Gupta S, Yadav BC, Dwivedi PK, Das B. Microstructural, optical and electrical investigations of Sb-SnO_2 thin films deposited by spray pyrolysis. *Materials Research Bulletin.* 2013;48(9): 3315-3322.
24. Frohlich D, Kezklies R. Band-Gap Assignment in SnO_2 by Two-Photon Spectroscopy. *Phys. Rev. Lett.* 1978;41(25): 1750.
25. Roth AP, Williams DF. Properties of zinc oxide films prepared by the oxidation of diethyl zinc. *Journal of Applied Physics.* 1981;52(11): 6685-6692.
26. Fauzia V, Yusnidar MN, Hanum Lalasari L, Subhan A, Umar AA. High figure of merit transparent conducting Sb-doped SnO_2 thin films prepared via ultrasonic spray pyrolysis. *Journal of Alloys and Compounds.* 2017;720: 79-85.
27. Zheng H, Li L, Sun Z, Yu S, Luo W. Preferential orientation, microstructure and functional properties of SnO_2:Sb thin film: the effects of post-growth annealing. *Appl. Surf. Sci*. 2016;362: 230-236.
28. Yang W, Yu S, Zhang Y, Zhang W. Properties of Sb-doped SnO_2 transparent conductive thin films deposited by radio-frequency magnetron sputtering. *Thin Solid Films.* 2013;542: 285-288.
29. Rana MPS, Singh F, Joshi K, Negi S, Ramola RC. Influence of electronic excitations on structural, optical and electrical properties of undoped and antimony doped tin oxide thin films. *Thin Solid Films.* 2016;616: 34-42.
30. Feng G, Shu Fen W, Meng Kai L, Xiu Feng C, Su Wen L, Guang Jun Z, Dong X, Duo Rong Y, Luminescence of SnO_2 thin films prepared by spin-coating method. *Journal of Crystal Growth.* 2004;262: 182-185.
31. Patil LA, Shinde MD, Bari AR, Deo VV. Highly sensitive and quickly responding ultrasonically sprayed nanostructured SnO_2 thin films for hydrogen gas sensing. *Sensors and Actuators B.* 2009;143(1): 270-277.
32. Wenhao Y, Shihui Y, Yang Z, Weifeng Z. Properties of Sb-doped SnO_2 transparent conductive thin films deposited by radio-frequency magnetron sputtering. *Thin Solid Films.* 2013; 542: 285-288.
33. Tauc J, Grigorovici R, Vancu A. Optical Properties and Electronic Structure of Amorphous Germanium. *Phys. Status Solidi.* 1996;15: 627.
34. Urbach F. The long-wavelength edge of photographic sensitivity and of the electronic absorption of solids. *Phys. Rev.* 1953;92(5): 1324.
35. Yuheng W, Jin M, Feng J, Xuhu Y, Honglei M, Structural and photoluminescence characters of SnO_2:Sb films deposited by RF magnetron sputtering. *Journal of Luminescence.* 2005;114(1): 71-76.
36. Kim TW, Lee DU, Yoon YS. Microstructural, electrical, and optical properties of SnO_2 nanocrystalline thin films grown on InP (100) substrates for applications as gas sensor devices. *Journal of Applied Physics.* 200;88(6): 3759.
37. Shinde SS, Shinde PS, Sathe VG, Barman SR, Bhosale CH, Rajpure KY. Electron–phonon interaction and size effect study in catalyst based zinc oxide thin films. *J. Mol. Structure.* 2010;984(1-3): 186.

38. Babar AR, Shinde SS, Moholkar AV, Bhosale CH, Kim JH, Rajpure KY. Sensing properties of sprayed antimony doped tin oxide thin films: solution molarity. *J. Alloys Compd.* 2011;509(6): 3108-3115

THE AUTHORS

Habieb H.
e-mail: habieb.halima@gmail.com
ORCID: 0000-0003-3952-8198

Hamdadou N.
e-mail: nasreddine.hamdadou@enp-oran.dz
ORCID: 0000-0003-1880-6881